# MAPS: constraining serendipitous time variability in protoplanetary disk molecular ion emission

Waggoner, A.R.; Cleeves, L.I.; Loomis, R.A.; Aikawa, Y.; Bae, J.; Bergner, J.B.; … ; Wilner, D.J.

# MAPS: Constraining Serendipitous Time Variability in Protoplanetary Disk Molecular Ion Emission

Abygail R. Waggoner[1] , L. Ilsedore Cleeves[1] , Ryan A. Loomis[2] , Yuri Aikawa[3] , Jaehan Bae[4] , Jennifer B. Bergner[5] ,
Alice S. Booth[6] , Jenny K. Calahan[7] , Gianni Cataldi[3,8] , Charles J. Law[9] , Romane Le Gal[10,11] , Feng Long[12,14] ,
Karin I. Öberg[9] , Richard Teague[9,13] , and David J. Wilner[9]

[1] University of Virginia, Charlottesville, VA 22904, USA; arw6qz@virginia.edu
[2] National Radio Astronomy Observatory, 520 Edgemont Rd., Charlottesville, VA 22903, USA
[3] Department of Astronomy, Graduate School of Science, The University of Tokyo, Tokyo 113-0033, Japan
[4] Department of Astronomy, University of Florida, Gainesville, FL 32611, USA
[5] UC Berkeley Department of Chemistry, Berkeley, CA 94720, USA
[6] Leiden Observatory, Leiden University, 2300 RA Leiden, The Netherlands
[7] Department of Astronomy, University of Michigan, 323 West Hall, 1085 South University Ave., Ann Arbor, MI 48109, USA
[8] National Astronomical Observatory of Japan, Osawa 2-21-1, Mitaka, Tokyo 181-8588, Japan
[9] Center for Astrophysics, Harvard & Smithsonian, 60 Garden St., Cambridge, MA 02138, USA
[10] University Grenoble Alpes, CNRS, IPAG, F-38000 Grenoble, France
[11] IRAM, 300 rue de la Piscine, F-38406 Saint-Martin d'Hères, France
[12] Lunar and Planetary Laboratory, University of Arizona, Tucson, AZ 85721, USA
[13] Department of Earth, Atmospheric, and Planetary Sciences, Massachusetts Institute of Technology, Cambridge, MA 02139, USA

## Abstract

Theoretical models and observations suggest that the abundances of molecular ions in protoplanetary disks should be highly sensitive to the variable ionization conditions set by the young central star. We present a search for temporal flux variability of $HCO^+$ $J = 1$–$0$, which was observed as a part of the Molecules with Atacama Large Millimeter/submillimeter Array (ALMA) at Planet-forming Scales ALMA Large Program. We split out and imaged the line and continuum data for each individual day the five sources were observed (HD 163296, AS 209, GM Aur, MWC 480, and IM Lup, with between three and six unique visits per source). Significant enhancement ($>3\sigma$) was not observed, but we find variations in the spectral profiles in all five disks. Variations in AS 209, GM Aur, and HD 163296 are tentatively attributed to variations in $HCO^+$ flux, while variations in IM Lup and MWC 480 are most likely introduced by differences in the $uv$ coverage, which impact the amount of recovered flux during imaging. The tentative detections and low degree of variability are consistent with expectations of X-ray flare-driven $HCO^+$ variability, which requires relatively large flares to enhance the $HCO^+$ rotational emission at significant ($>20\%$) levels. These findings also demonstrate the need for dedicated monitoring campaigns with high signal-to-noise ratios to fully characterize X-ray flare-driven chemistry.

*Unified Astronomy Thesaurus concepts:* Astrochemistry (75); Protoplanetary disks (1300); Pre-main-sequence stars (1290); Radio astronomy (1338); Stellar flares (1603); Stellar X-ray flares (1637); Young stellar objects (1834); Radio spectroscopy (1359)

## 1. Introduction

Molecular abundances within protoplanetary disks have traditionally been expected to evolve over tens to hundreds of thousands of years or longer (Henning & Semenov 2013; Öberg & Bergin 2021, and references therein). However, young pre-main-sequence stars at the center of disks are active in the X-ray regime on timescales of days to weeks (e.g., Getman et al. 2005, 2022a, 2022b; Wolk et al. 2005). Due to an unstable dynamo, young stars regularly undergo magnetic reconnection events that result in a larger burst of X-ray photons commonly known as an X-ray flare (Güdel 2004, and references therein), which can temporarily increase the X-ray flux and disk ionization rates (Ilgner & Nelson 2006a). Flares can range in strength, increasing the flux by a factor of a few to

several hundred times the baseline flux (Getman et al. 2005; Getman & Feigelson 2021).

Flare-driven variable ionization rates drive variability in chemical species in disks. This variation largely stems from time variability in the ionization of $H_2$ and He, which play a major role in driving cold molecular chemistry (Maloney et al. 1996). For example, a single strong flare (i.e., 100 times stronger than the baseline luminosity) can temporarily increase the abundance of $H_2^+$ by up to a factor of $\sim70$. $H_2^+$ then forms $H_3^+$, which enhances the formation of gas-phase species, such as $H_2O$, near the disk surface ($<100$ au from the central star; Waggoner & Cleeves 2019). Gas-phase cations are especially sensitive to flares, where some species, such as $HCO^+$ and $N_2H^+$, can be increased by several orders of magnitude for days or weeks, depending on the strength of the flare. For example, Waggoner & Cleeves (2022) found that a single strong flare can increase the disk-integrated abundance of $HCO^+$ and $N_2H^+$ by $\sim4$ and $\sim3$, respectively. Additionally, the cumulative effect of thousands of flares aids in the advancement of chemical complexity over the course of hundreds of years by marginally ($\sim1\%$ change) increasing

---

[14] NASA Hubble Fellowship Program Sagan Fellow.

**Table 1**
The R.A., decl., Systemic Velocity, Number of Unique Observation Days, Minimum Baseline Used for Imaging, and Beam Size for Each of the Five MAPS Disks

| Source | R.A. (J2000) | Decl. | Sys. Vel. (LSRK, km s$^{-1}$) | Num. of Obs. | Min. Baseline (m) | Beam (arcsec) | BPA |
|---|---|---|---|---|---|---|---|
| IM Lup | 15: 56: 09.186780 | −37.56.06.58091 | 4.5 (6) | 3 | 60 | 2.0 | 63.8 |
| GM Aur | 04: 55: 10.981558 | +30.21.58.87742 | 5.6 (4) | 5 | 55 | 2.0 | 8.6 |
| AS 209 | 16: 49: 15.293780 | −14.22.09.09404 | 4.6 (3) | 5 | 50 | 2.0 | 62.4 |
| HD 163296 | 17: 56: 21.277330 | −21.57.22.63945 | 5.8 (1), (2) | 6 | 70 | 2.0 | 76.3 |
| MWC 480 | 04: 58: 46.274800 | +29.50.36.47709 | 5.1 (2), (5) | 5 | 50 | 2.2 | 16.7 |

**Notes.** For each disk, the beam was tapered and smoothed to be circular and the same across all epochs. The minimum baseline is the smallest baseline coverage used in the imaging process.
**References.** (1) Teague et al. 2019; (2) Teague et al. 2021; (3) Huang et al. 2017; (4) Huang et al. 2020; (5) Piétu et al. 2007; (6) Pinte et al. 2018.

the production of carbon chains and organosulphides (Waggoner & Cleeves 2022).

While this study is motivated specifically by flare-driven variable ionization rates, it is important to note that other processes can drive variability. For example, accretion outbursts are known to increase UV flux and disk temperature. Observations and models indicate that outbursts evaporate ices and increase gas density, which in turn drives chemical reactions (e.g., Molyarova et al. 2018; Kóspál et al. 2021; Leemker et al. 2021; Fischer et al. 2022; Ruíz-Rodríguez et al. 2022; Tobin et al. 2023).

Significant enhancement in the flux of a gas-phase cation has been reported previously by Cleeves et al. (2017) in observations of the H$^{13}$CO$^+$ $J = 3-2$ line with the Atacama Large Millimeter/submillimeter Array (ALMA). Cleeves et al. observed H$^{13}$CO$^+$ $J = 3-2$ in the IM Lup protoplanetary disk on three separate days: 2014 July, 2015 January, and 2015 May. In 2014 July and 2015 January, the H$^{13}$CO$^+$ flux was effectively constant, but in 2015 May the flux doubled (an increase of 28$\sigma$). They concluded that enhancement was not caused by an increase in temperature, as the continuum emission remained constant, thus ruling out an outburst or similar type event. IM Lup, like most young stars, is known to be X-ray variable (Cleeves et al. 2017). Indeed, the most likely source of H$^{13}$CO$^+$ enhancement was due to an X-ray flaring event.

In fact, the detection in IM Lup was serendipitous and is currently the only source with reported variability. Espaillat et al. (2022) searched for variations in CO millimeter emission in GM Aur; however, no significant variability was seen. This result was somewhat expected, since chemical models in Espaillat et al. (2022) and in Waggoner & Cleeves (2022) indicate that the robust CO molecule is not sensitive to variable X-ray and UV ionization rates.

This work seeks evidence of flare-driven chemistry by searching for variability of the HCO$^+$ $J = 1-0$ line in the five disks, HD 163296, AS 209, GM Aur, MWC 480, and IM Lup, observed as a part of the Molecules with ALMA at Planet-forming Scales (MAPS) ALMA Large Program (Öberg et al. 2021), which fortuitously was observed at multiple dates spanning about a year. Section 2 describes the observational setup, sources, and line selection. Section 3 describes the CLEANing strategy, methodology, and error analysis. The results are presented in Section 4, where the degree of variability is constrained. In Section 5, we discuss the presence/absence of variability, along with possible connections to X-ray flaring events and/or related variable ionization rates. Section 6 provides a summary of this work along with concluding remarks.

## 2. Observations

The data used in this work were taken as a part of the MAPS ALMA Large Program (2018.1.01055.L; Öberg et al. 2021). MAPS observations included five sources: the IM Lup, GM Aur, AS 209, HD 163296, and MWC 480 protoplanetary disks. Table 1 includes the coordinates, systemic velocity, and additional observation details for each disk. MWC 480 and HD 163296 are both Herbig Ae systems, while the other three are T Tauri systems. These five disks were selected because they are bright and chemically rich, thus allowing for more in-depth observations (for more details, see Section 2.1 of Öberg et al. 2021).

HCO$^+$ $J = 1-0$ observations were carried out between 2018 October and 2019 September, where short-baseline data were collected in 2018 October and December and long-baseline data were taken in 2019 August and September. Table 2 provides the baseline coverage and integrated observation time for each observation of each disk. Detailed descriptions of the data collection and the data reduction analysis are provided in Öberg et al. (2021) and Czekala et al. (2021), respectively.

For the most part, there was only a single execution per observation day, with the exceptions of MWC 480 and GM Aur. Both of these sources were observed twice on 2019 September 2. A 1 day separation was found to be the optimal time to split the data based on (1) timing of the execution blocks, (2) optimizing the signal-to-noise ratio (S/N) of the data, and (3) providing the maximum number of distinct observations possible to search for variability.

For this work, we chose to limit the data to HCO$^+$ 1–0 taken as a part of MAPS. There are previous observations of emission lines of HCO$^+$ and its various isotopes in the MAPS sources. However, by limiting the analysis to MAPS data, the analysis is much more homogeneous and allows for a more robust comparison between observations.

### 2.1. Line Selection

We use Band 3 data of HCO$^+$ $J = 1-0$ (89.188525 GHz) for each of the five MAPS disks. HCO$^+$ was found to be the most likely candidate to trace variable disk chemistry based on models used in Waggoner & Cleeves (2022), as gas-phase cations have been shown to be the most susceptible to variable ionization rates. Aikawa et al. (2021) found that the optical depth ($\tau$) of the HCO$^+$ line is ∼1 for each of the MAPS disks. While a more optically thin line would be more ideal for this study, HCO$^+$ 1–0 is the only gas-phase cation that is sufficiently bright to allow splitting into individual images for each observation block.

**Table 2**
The Baseline Coverage (*uv*) and Total Observation Time Spent on Source for Each Observation Day for Each Disk

| Source | Date | *uv* (m) | Time (s) |
|---|---|---|---|
| IM Lup | 2018 Oct 29 | 13.5–1258.6 | 2470.90 |
| | 2019 Aug 20 | 35.7–3188.1 | 3751.49 |
| | 2019 Aug 21 | 39.2–3506.6 | 3698.02 |
| GM Aur | 2018 Dec 13 | 12.7–667.3 | 2372.98 |
| | 2018 Dec 15 | 12.0–687.8 | 2345.52 |
| | 2019 Aug 31 | 22.7–3143.7 | 3976.56 |
| | 2019 Sep 2 | 24.4–3141.3 | 8548.70 |
| | 2019 Sep 4 | 25.7–2904.0 | 4218.82 |
| AS 209 | 2018 Oct 26 | 14.3–1394.8 | 2520.43 |
| | 2019 Aug 23 | 39.9–3396.5 | 3660.77 |
| | 2019 Aug 24 | 31.6–3330.3 | 3612.77 |
| | 2019 Sep 3 | 70.5–3118.4 | 3666.29 |
| | 2019 Sep 4 | 27.7–3627.5 | 3641.57 |
| HD 163296 | 2018 Oct 22 | 12.7–1347.6 | 2511.17 |
| | 2019 Aug 23 | 56.7–2742.3 | 3503.42 |
| | 2019 Aug 24 | 30.3–3335.1 | 3499.78 |
| | 2019 Aug 25 | 39.1–3389.0 | 3519.79 |
| | 2019 Sep 4 | 34.6–3071.5 | 3508.90 |
| | 2019 Sep 5 | 73.0–3637.1 | 3527.23 |
| MWC 480 | 2018 Dec 13 | 12.0–671.2 | 2974.51 |
| | 2018 Dec 15 | 12.1–691.7 | 2931.70 |
| | 2019 Aug 31 | 23.0–3143.8 | 4141.15 |
| | 2019 Sep 2 | 24.7–3142.6 | 8573.71 |
| | 2019 Sep 4 | 26.1–2884.5 | 4245.26 |

**Note.** Each unique observation day was a single ALMA execution block, except 2019 September 2 in MWC 480 and GM Aur, which contain two execution blocks.

We investigated whether a similar analysis was possible for neutral species observed simultaneously with $HCO^+$; however, the $C_2H$ and HCN lines were too weak to split into individual observations. A search for minor spectral changes was not feasible, due to low S/Ns.

All data used in this work are publicly available directly on the ALMA archive or through the interactive MAPS website[15] (see also Section 3.5 in Öberg et al. 2021). The line measurement set, line mask, and line plus continuum measurement set can be downloaded directly from the MAPS website. Continuum masks were hand-drawn for each disk.

## 3. Methods

### 3.1. CLEANing Strategy

The line and continuum are imaged using the same process starting with the measurement sets (described in Section 2) using CASA version 6.2, where the line is flagged from the line plus continuum measurement set to generate the continuum image. Line images are produced using the briggsbwtaper weighting with a robust value of 0.5. briggsbwtaper is new to CASA as of version 6.2 and handles gridding more accurately than the commonly used briggs weighting. All images are CLEANed to $3\sigma$, where $\sigma$ is the rms measured in the dirty image. The imaging process proceeds as follows:

1. Data for each observation day are split into a new measurement set using the function split in CASA. Data taken on individual days are not further split because sensitivity would drastically decrease. Additionally, a day has been found to be sufficient time for a flare to occur between epochs (for flare statistics, see Wolk et al. 2005).
2. A dirty image is generated to determine the CLEANing threshold and dirty beam size.
3. A *uv* taper is estimated from

$$b_{tap} = \left( \frac{b_{dirty}^{-1} - b_{des}^{-1}}{(b_{dirty}^{-2} - b_{des}^{-2})^{0.5}} \right)^{-1}, \qquad (1)$$

where $b_{tap}$ is the *uv* taper, $b_{dirty}$ is the dirty beam, and $b_{des}$ is the desired beam size. The taper is unique for each observation execution, but the same taper is used for both line and continuum imaging. The taper is essential to generate a uniform, approximately circular beam size (the "target beam"; see Table 1) for each disk. Without a uniform beam, images for individual days could not be directly compared.

4. The lower-resolution images made by applying the taper to the visibilities are CLEANed using the MAPS mask presmoothed to a larger beam to encompass all of the line emission. The MAPS mask is used to select the CLEANed region; however, the mask is presmoothed to the new, larger beam to encompass the full flux of the lower-resolution line image. Smoothing is carried out with the CASA function imsmooth.
5. The CLEANed beam is nearly circular from the *uv* taper, but not perfectly. The final image is then smoothed using imsmooth to generate a uniform beam size and shape for each disk (listed in Table 1).

The CLEANing scripts are available upon request from A.R.W.

Figure 1 shows the moment-zero maps for all observations, which show integrated line emission. In this case, the moment-zero maps were generated by integrating flux across frequency space across the entire image cube. Maps were generated without use of the mask. Figure 2 shows the continuum images for each observation.

### 3.2. Flux and Error Analysis

The integrated flux for the continuum emission was determined by integrating all emission within the hand-drawn mask in the continuum image (Figure 2). The integrated flux was found by integrating all channels with significant flux. Channels containing the line were defined as any channel that contain data emission greater than $3\sigma$, where $\sigma$ was the standard deviation of the unmasked data in each channel.

The error for the integrated line flux ($F_{HCO^+}$) was determined as follows. First, the mask was randomly shifted to 40 different locations off source. The error of the integrated flux was then found by taking the standard deviation of the integrated flux within the off-source locations. The error for the integrated continuum flux ($F_{cont}$) was found in a similar manner. This sampling method was used, rather than shifting the mask to line free channels, due to the limited number of channels available in the MAPS products' measurement sets. The flux calibration error is <20% for all sources, with the assumption that the continuum flux should be constant across all observations (Figures 3–7). Flux calibration error ∼10% or greater is consistent with the ALMA technical handbook (Cortes et al. 2022).
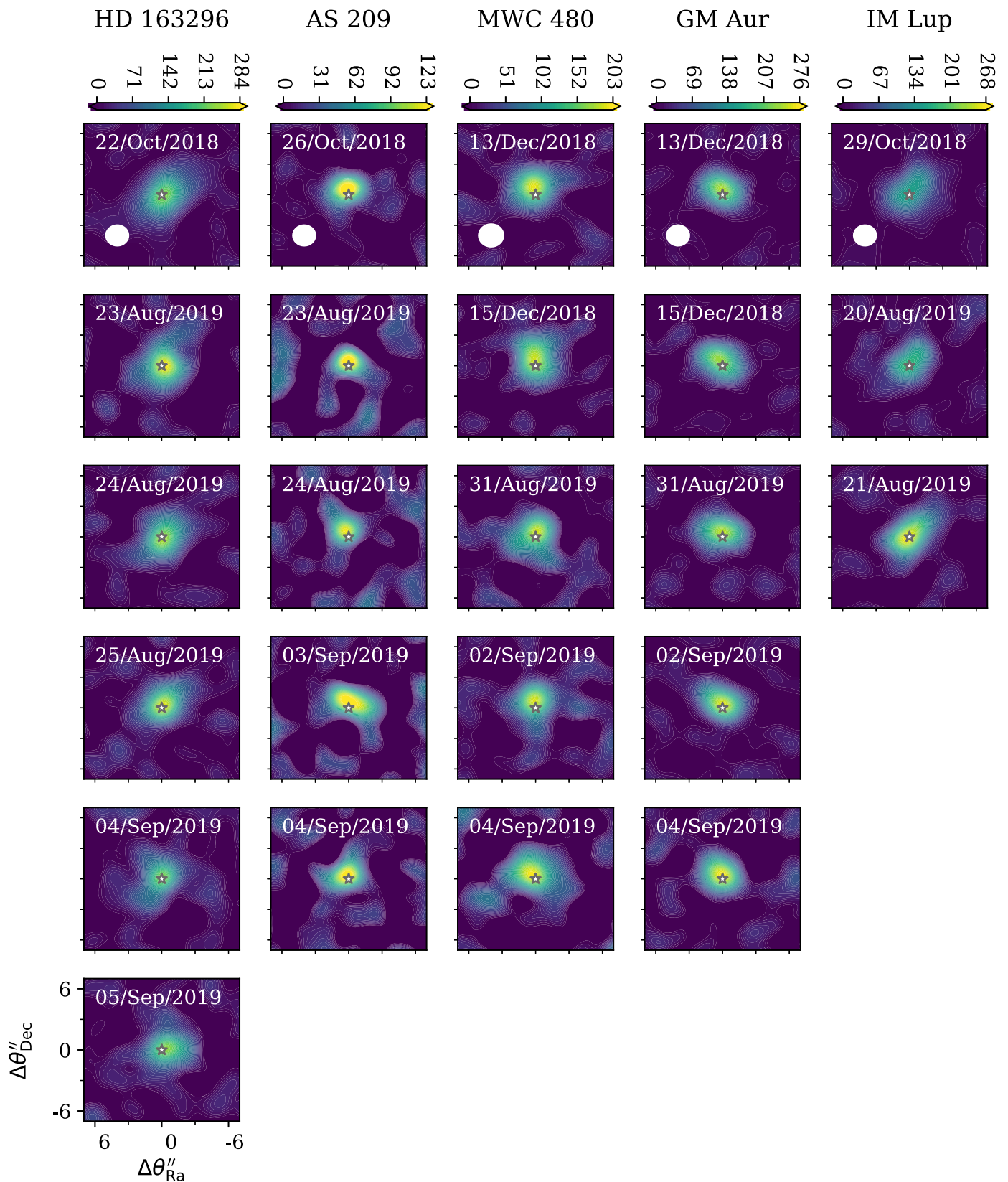
**Figure 1.** The moment-zero map of HCO$^+$ 1–0 for each observation execution for each disk. Each column corresponds to a different disk, while each row represents a separate observation day. The date of observation is shown in the top of each plot. Each disk has its own unique color bar with units in mJy. The beam for each disk is shown in white in the bottom left of the top row of images.

To ensure that any changes in HCO$^+$ emission were not due to changes in source brightness or temperature, the ratio of line flux to continuum flux ($F_{HCO^+}/F_{cont}$) was used to compare line brightness for individual observation days. The continuum is expected to be constant, just as it was observed to be for the IM Lup disk in Cleeves et al. (2017).
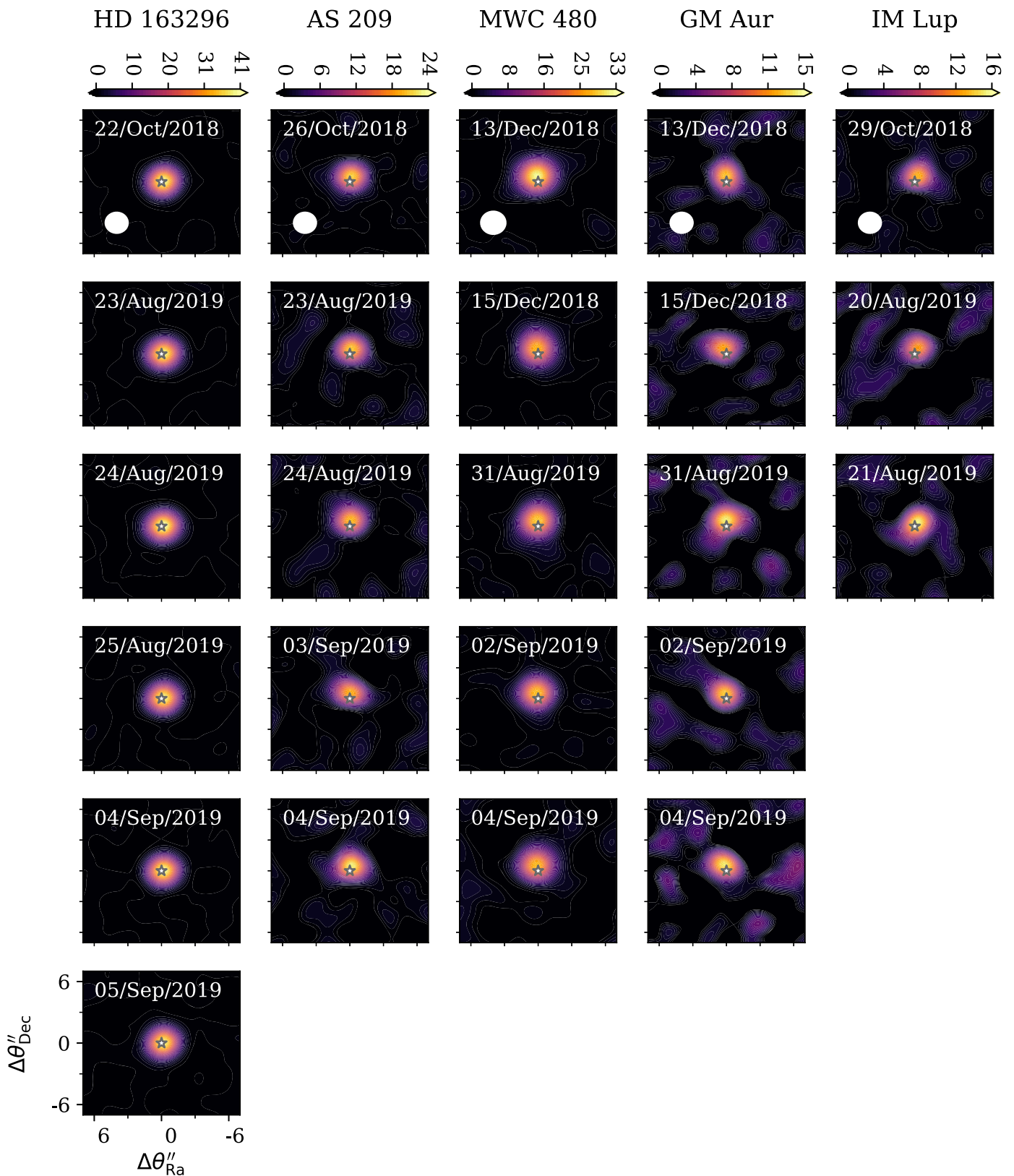
**Figure 2.** The 90 GHz continuum emission for each observation execution for each disk. Each column corresponds to a different disk, while each row represents a separate observation day. The date of observation is shown in the top of each plot. Each disk has its own unique color bar with units in mJy. The beam for each disk is shown in white in the bottom left of the top row of images.

### 3.3. Baseline Coverage

Interferometrically measured flux is inherently sensitive to the baseline coverage of the observation. Shorter baselines are known to probe flux better, while being less sensitive to structure, and longer baselines probe structure well, while being less sensitive to flux (for example, see Chapter 5 in
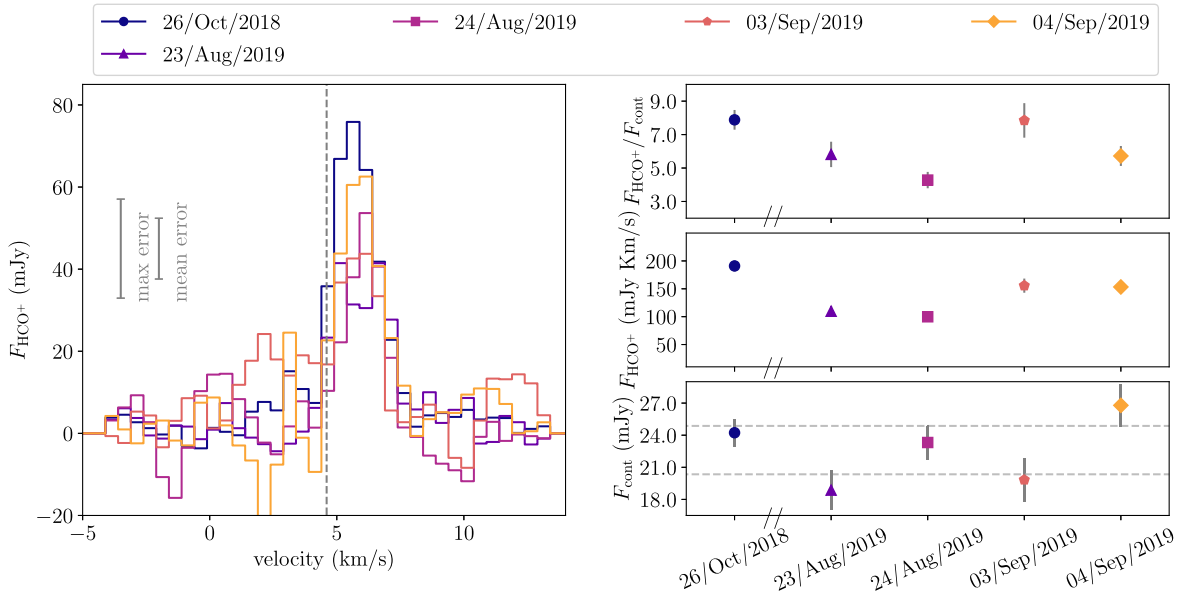
**Figure 3.** Left: the HCO$^+$ $J = 1-0$ spectra in the AS 209 disk for each unique observation day. The gray bars on the left represent the maximum and mean error (standard deviation) for all channels across all observations. Appendix B shows the spectra with error bars on each channel. Right: the disk-integrated continuum flux ($F_{cont}$, bottom), disk-integrated HCO$^+$ 1–0 flux ($F_{HCO^+}$, middle), and normalized line flux with respect to the continuum ($F_{HCO^+}/F_{cont}$, top) for each day HCO$^+$ 1–0 was observed in AS 209. Units for $F_{HCO^+}/F_{cont}$ are mJy km s$^{-1}$ mJy$^{-1}$. Error bars indicate $1\sigma$. Gray dashed lines in the bottom plot indicate $\pm 10\%$ of the average continuum flux.
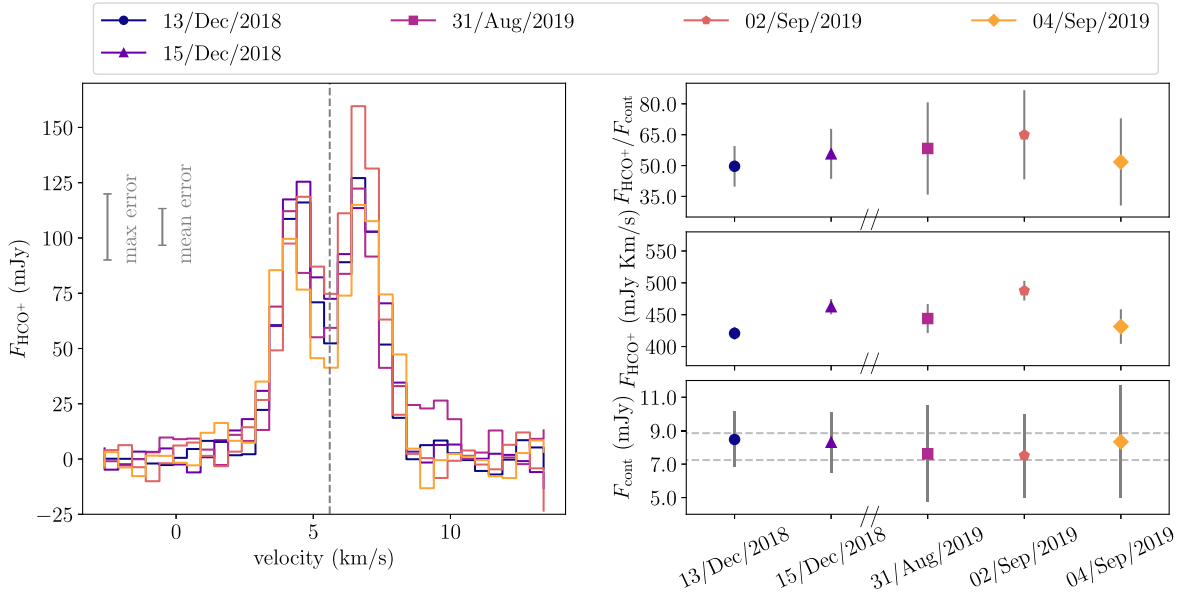


**Figure 4.** Same figure description as Figure 3, but for GM Aur.

Thompson et al. 2017). The MAPS observations utilized multiple ALMA configurations to optimize the baseline coverage to include both short and long baselines. While this method is incredibly useful in generating a complete picture of the disk across multiple scales, varying telescope configurations adds an additional challenge to compare flux on different observation days.

Observations with longer-baseline coverage, i.e., fewer short baselines, miss flux on larger scales (Thompson et al. 2017). A minimum baseline distance was set for each disk to ensure that long-baseline observations do not have an artificially lower flux than images with thorough short-baseline coverage. Even though the most "flux sensitive" baselines were removed, there is still sufficient *uv* sampling across all epochs to cross-compare them.

A range of minimum baseline values were examined, and we selected values that preserved as many short baselines as possible consistently across different epochs without cutting out too many short baselines and thereby introducing imaging artifacts (listed in Table 1). On average, there was a 22% ± 12 loss in flux as a result of this process, based on comparisons between the clipped data and the full measurement set.

To further ensure that any detected variability was not artificially introduced by the varying baseline coverage, the PYTHON routine vis_sample[16] was used to create "mock"

---

[16] vis_sample is publicly available under the MIT license at https://github.com/AstroChem/vis_sample and described in further detail in Loomis et al. (2018).
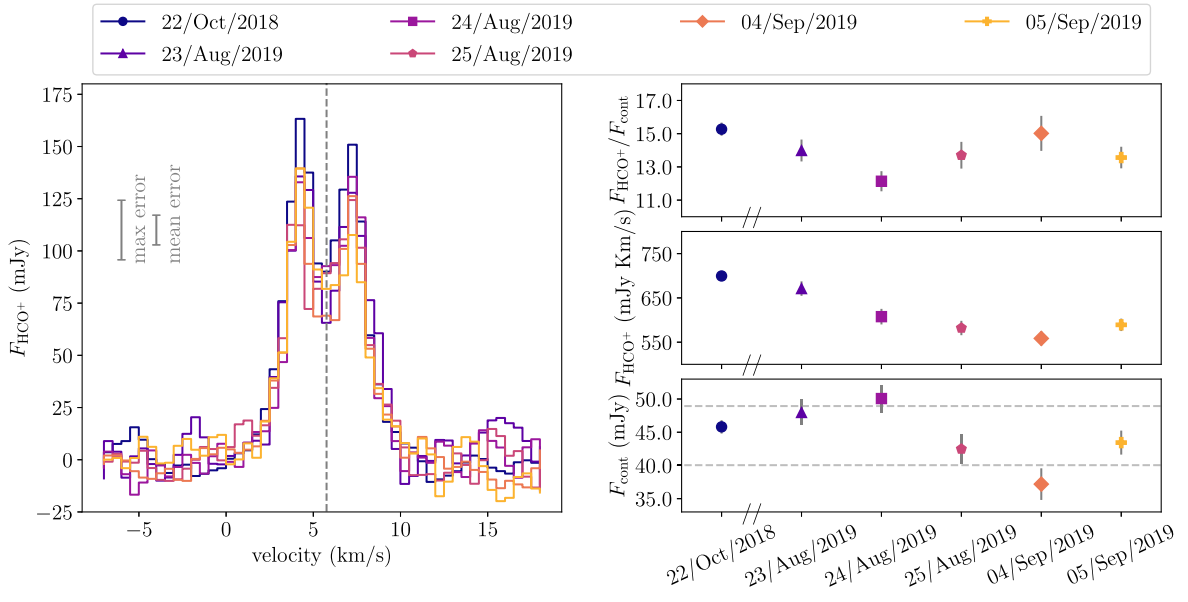
**Figure 5.** Same figure description as Figure 3, but for HD 163296.
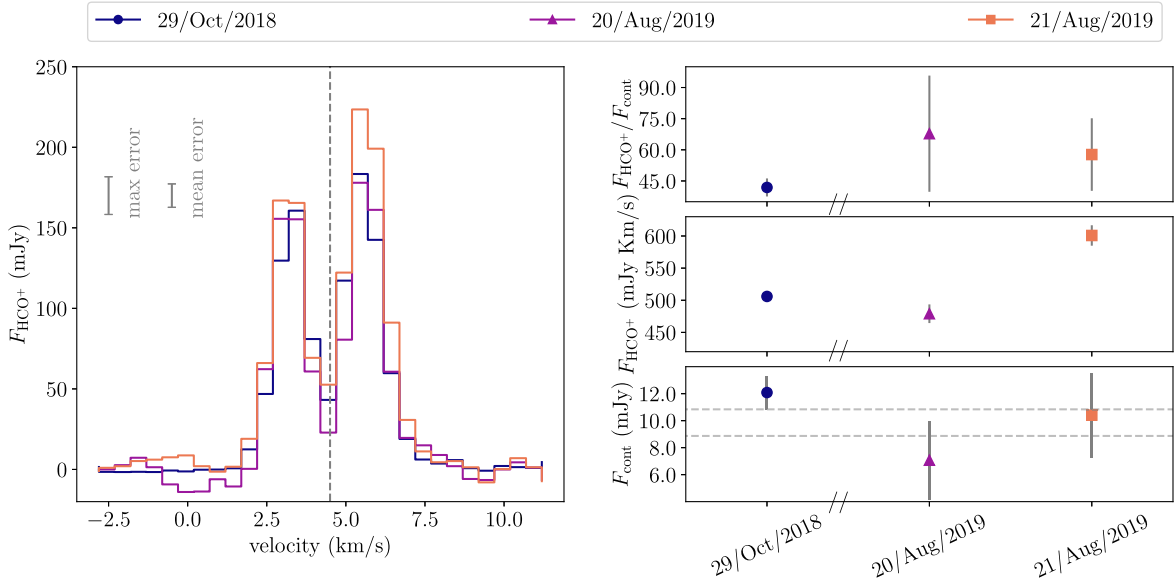


**Figure 6.** Same figure description as Figure 3, but for IM Lup.

data sets for each observation of each disk. The mock data were generated by first imaging the time-integrated images of $HCO^+$ $J = 1-0$ (i.e., the complete observation set), as was done by Aikawa et al. (2021). The time-integrated image is considered to be the "ground truth" to generate the mock data set. Synthetic ALMA observations were created by running the time-integrated image through `vis_sample` for each of the observation days. This generated a synthetic observation using the same visibility effects as the actual observation. Mock images were created by imaging the synthetic observations using the same `CLEAN`ing process used for the real data (described above). This process helps constrain variability in $HCO^+$ or continuum emission introduced by visibility (i.e., *uv* sampling) effects, but the possibility of visibility effects is still considered in the results.

## 4. Results

### 4.1. General Behavior

A variable source is defined as any source with at least one observation where there is a $\geqslant 3\sigma$ change in disk-integrated $F_{HCO^+}/F_{cont}$. A tentatively variable source is defined as a source with at least one observation day that has variability in the $HCO^+$ $J = 1-0$ intensity spectrum. Spectral variability is defined on a case-by-case basis in the following sections. In this work, all changes in spectral shape are considered tentative due to (relatively) low S/Ns. A tentatively variable source does not display variations in the disk-integrated $F_{HCO^+}$, $F_{cont}$, and $F_{HCO^+}/F_{cont}$, i.e., all integrated flux values are within $3\sigma$ of each other. All tentative variability occurs on a channel-by-channel basis.
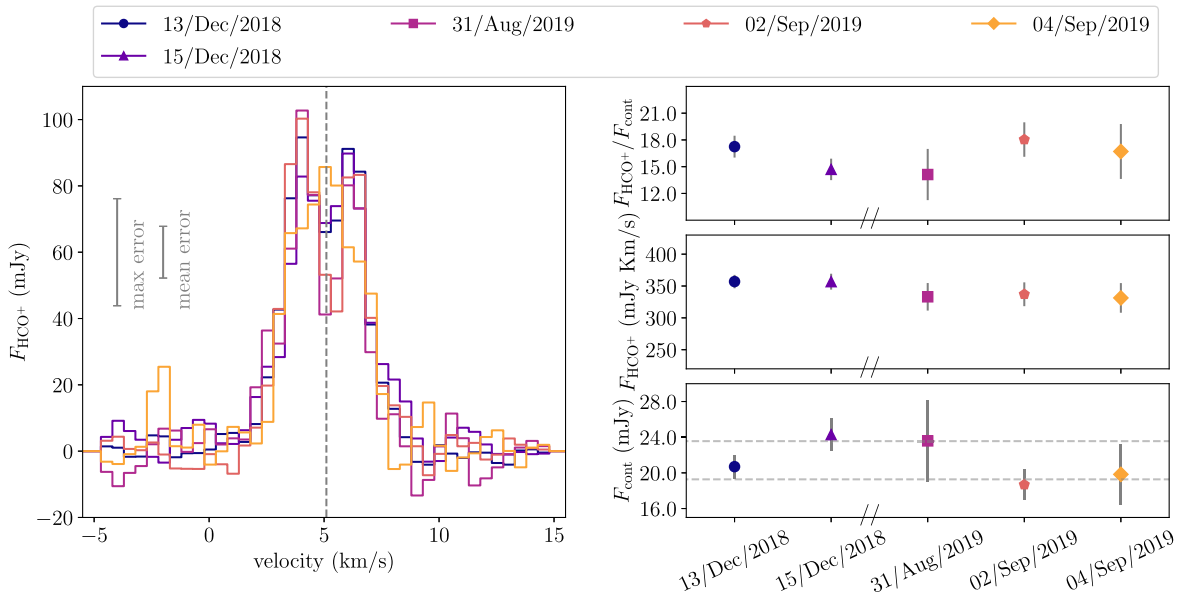
**Figure 7.** Same figure description as Figure 3, but for MWC 480.

None of the five disks were found to be variable on a disk-integrated basis in HCO$^+$ $J = 1-0$ emission during the MAPS observations, as is clear in the moment-zero maps (Figure 1), which are constant within the error bars across nearly all epochs. On 2019 September 3, the disk-integrated HCO$^+$ line flux observed in the AS 209 disk has more of an oval shape compared to the other epochs, which are more circular. This morphological difference appears to be a result of a small excess of blueshifted emission on 2019 September 3 compared to the other days (discussed further in Section 4.3). On 2019 August 21, HCO$^+$ emission in IM Lup is brighter than the other epochs. However, our analysis suggests the brighter line flux is likely caused by differences in baseline coverage (discussed further in Section 4.6).

While the disk-integrated flux remained constant within the error bars for all disks, we report tentative variability in three of the five disks: AS 209, GM Aur, and HD 163296. Each of these disks features some form of variability or shift in the HCO$^+$ spectral shape, as further discussed below (Sections 4.3, 4.4, and 4.5). MWC 480 also displays a shift in the HCO$^+$ spectral shape, but this shift is at the level of the noise (Section 4.7). IM Lup has a brighter peak at 6.8 km s$^{-1}$ than other observation days, but the higher flux is most likely caused by baseline coverage (Section 4.6). Noise on a channel-by-channel basis is further discussed in Appendix B.

As discussed in Section 3.3 and Appendix A, we investigate if the differences in baseline coverage impact the measured flux. A "known flux" model was created using `vis_sample`. The analysis suggests that the tentative HCO$^+$ spectral variability in AS 209, GM Aur, and HD 163296 was unlikely to be introduced by differences in baseline coverage at the level of the noise in the data. However, IM Lup and MWC 480 appear to have been impacted by these effects.

### 4.2. Continuum

There are no significant and distinguishable differences in the continuum images taken as a part of the MAPS observation set (Figure 2). For each disk, disk-integrated $F_{cont}$ values (taking into account rms uncertainty) were within $10\% \sim 20\%$ of each other. This magnitude of variation is consistent with the acceptable level of flux calibrator uncertainty reported for ALMA (Francis et al. 2020; Cortes et al. 2022). Therefore, all observations of continuum emission are constant within error for all disks.

While a clear ($>3\sigma$) change in integrated flux is not seen, the spectral peak at 6.1 km s$^{-1}$ relative to the source velocity is $\sim62\%$ higher on 2018 October 26 compared to the other observation days. Additionally, the emission peak shifts toward the source velocity by $\sim5.1$ km s$^{-1}$, or by one channel, on 2018 October 26. Notably, 2018 October has the best short-baseline coverage, and the increase in emission and peak shift could be attributed to higher sensitivity to extended emission on this date.

There is also some variability in the wings, notably on 2019 September 3 where a higher flux is seen at 12.1 and 1.6 km s$^{-1}$. Emission at 1.6 km s$^{-1}$ is significant because this is the only day that blueshifted emission is detected for any of the observed dates. While it is difficult to say with certainty, there is a slight elongation in the moment-zero maps (Figure 1) on this day compared to the other dates. The channel maps showed that the excess emission was centrally peaked.

Changes in the spectrum are considered tentative, and a higher S/N is required to confirm if the general variable behavior of this source is indeed real or a noise artifact.

### 4.3. AS 209

AS 209 is the faintest source in HCO$^+$ 1–0 of the five disks (Figure 3). Previous observations have revealed a cold molecular cloud in the foreground of AS 209, and the cloud absorbs cold emission from AS 209 at select velocities in CO gas (Öberg et al. 2011; Huang et al. 2016; Favre et al. 2019) and in HCO$^+$ gas (Law et al. 2021). In this source, HCO$^+$ 1–0 is considered to be tentatively variable over the MAPS observations.

### 4.4. GM Aur

HCO$^+$ 1–0 is considered tentatively variable in GM Aur, due to slight variations on 2019 August 31 (Figure 4). On this day,

peak $F_{\mathrm{HCO^+}}$ at $6.6\,\mathrm{km\,s^{-1}}$ is $\sim 25\%$ higher than the other epochs. The peak at $4.6\,\mathrm{km\,s^{-1}}$ remains constant across all observations. On 2019 September 2, a shoulder is visible at $9.6\,\mathrm{km\,s^{-1}}$ that is not seen on the other observation days.

Notably, both occurrences of variability are asymmetric, where channels within the redshifted portion of the spectrum are enhanced while the blueshifted side of the spectrum remains constant. The complex substructure observed in GM Aur may be the force behind asymmetric variations. As a flare propagates through the disk, light could be asymmetrically scattered due to spiral arms, which were seen in $^{12}$CO gas emission (Huang et al. 2021). However, spiral arms were not seen in $\mathrm{HCO^+}$ emission, which indicates that the substructure of GM Aur is complex. Without further modeling, it is uncertain how exactly the spiral arms would influence flare propagation or chemical changes.

### 4.5. HD 163296

HD 163296 is considered tentatively variable in $\mathrm{HCO^+}$ 1–0 emission (Figure 5). On 2018 October 22 (the first epoch), the double peaks are symmetrically $\sim 15\%$ higher than the following observations. This change is small, symmetric, and only occurs on one day, so calibration or baseline effects could have introduced the variation. While steps were taken to minimize variations introduced by baseline coverage (Section 3.3), the 2018 October observation has more complete low-baseline coverage than the later observations. While steps were taken to minimize variations introduced by baseline coverage, this epoch was the most impacted by flux loss. There was a 42% loss of flux on this day when small baselines were removed, which indicates that the 2018 October observation was strongly impacted by visibility effects. This sensitivity indicates that the enhancement could be caused by unaccounted visibilities. Even though our investigation of flux recovery did not suggest this to be true (Appendix A), the possibility is not ruled out.

### 4.6. IM Lup

Though significant variability was seen in $\mathrm{H^{13}CO^+}$ $J = 3$–2 in previous observations (Cleeves et al. 2017), the $\mathrm{HCO^+}$ 1–0 flux is observed to be relatively constant in this data set (Figure 6). The spectral peak at $6.8\,\mathrm{km\,s^{-1}}$ is $\sim 26\%$ higher on 2019 August 21 compared to other observations, which is also seen in the moment-zero maps (Figure 1). However, the fluctuation may be due to baseline coverage. Flux retrieval on a model of known flux (using `vis_sample`) shows the same spectral variation, suggesting that the increase in emission is introduced by differences in *uv* coverage (Appendix A).

IM Lup has slightly better low-baseline coverage than the other four sources, with 90% of baselines being $\geqslant 280\,\mathrm{m}$ for IM Lup and $\geqslant 310\,\mathrm{m}$ for all other sources. Additionally, IM Lup is the most extended source (gas emission up to $\sim 750$ au; Panić et al. 2009; Avenhaus et al. 2018) in the sample, thus the large-scale emission area is more sensitive to shorter baselines.

### 4.7. MWC 480

The disk-integrated $\mathrm{HCO^+}$ 1–0 line flux in MWC 480 is effectively constant during the MAPS observations (Figure 7). The line shape is a symmetric double-horned peak and the emission remains constant in flux and shape on all observation

days except 2019 September 4. On this day, the spectral shape becomes symmetrically singly peaked at the source velocity ($5.1\,\mathrm{km\,s^{-1}}$). The data from this day are noisier, with a lower S/N (see Appendix B), and therefore the single peak profile may be due to noise.

There is also a small blueshifted peak of emission at $-2.4\,\mathrm{km\,s^{-1}}$ only seen on 2019 September 4. The emission is present across two channels and has a peak significance of $\sim 5\sigma$ in disk-integrated line flux. Interestingly, a blueshifted peak was also seen in earlier observations of $\mathrm{HCO^+}$ 3–2 as a part of the Disk Imaging Survey of Chemistry with SMA survey (Öberg et al. 2010). At this time, the origin of this tentative enhancement in emission at $-2.4\,\mathrm{km\,s^{-1}}$ is unclear, although it could be due to a jet (Grady et al. 2010) or other similar phenomena.

## 5. Discussion

This work was motivated by models (Waggoner & Cleeves 2019, 2022) and observations (Cleeves et al. 2017) that suggest flare-driven variable X-ray ionization rates result in variable gas-phase cation abundances. In each of the five MAPS disks, some degree of spectral variation was seen in their $\mathrm{HCO^+}$ 1–0 emission. However, generally, the variations were small ($\lesssim 3\sigma$) and occurred within discrete parts of the spectrum rather than there being an overall increase in emission.

### 5.1. Possible Sources of Spectral Variability

The two most likely scenarios that could explain spectral variations seen in this work are as follows. First, observed changes in flux could be astrophysical, i.e., real variations in $\mathrm{HCO^+}$ emission. Second, the changes in measured line emission could be nonastrophysical and instead introduced as a result of the observing and/or imaging process. In this section, we discuss the possibility of both scenarios, and the observational consequences of each scenario.

#### 5.1.1. Possible Astrophysical Origins of Variability

In this discussion, we classify possible variability sources, but it should be noted that "types" of variability may not (and likely are not) exclusive to one another. In reality, variability in astronomical sources is incredibly dynamic, where bursts, flares, and other similar phenomena occur across the electromagnetic spectrum and can even include cosmic rays. For example, accretion outbursts increase both UV ionization rates and temperature (Molyarova et al. 2018), and X-ray flares are often associated with coronal mass ejections (Benz & Güdel 2010). Increased ionization rates driven by radiation are the most likely sources of the spectral changes we report.

X-ray flares are one possible source of variability in the $\mathrm{HCO^+}$ spectra. Waggoner & Cleeves (2019, 2022) indicate that changes in abundance scale directly with flare strength, where larger flares result in a higher and longer increase in $\mathrm{HCO^+}$ abundance than smaller flares. Relatively large X-ray flares (i.e., flares that increase the baseline X-ray luminosity by tens or hundreds) can increase the abundance of $\mathrm{HCO^+}$ by factors of two or more. Relatively small flares, also known as nano- or microflares (i.e., flares that increase baseline X-ray luminosity by a factor of a few; see Pearce & Harrison 1988; Feldman et al. 1997), result in a relatively small $\mathrm{HCO^+}$ enhancement. Radiative transfer models are required to know precisely how

flares of varying strengths impact the $HCO^+$ flux, so for the purpose of this discussion, we assume that flux scales directly with $HCO^+$ abundance.

According to Waggoner & Cleeves (2022), if a relatively large X-ray flare had occurred, a clear and distinguishable change would have been seen in the $HCO^+$ spectra. Previous observations of $H^{13}CO^+$ in the IM Lup protoplanetary disk support this: the $H^{13}CO^+$ flux roughly doubled ($28\sigma$; Cleeves et al. 2017) in one observation compared to two others. Since all instances of (tentative) variation seen in this work are relatively small ($<3\sigma$), a strong flare is unlikely to be the source of variation. However, a relatively small flare, such as a nano- or microflare, would drive relatively small increases in the $HCO^+$ spectrum. Therefore, if the spectral changes reported in this work were caused by an X-ray flare, they are most likely to have been caused by a relatively small flare.

T Tauri stars, such as AS 209, GM Aur, and IM Lup are known to be X-ray bright and variable (Güdel et al. 2003), thus suggesting that, if the fluctuations are true changes in $HCO^+$ emission, they are most likely to be caused by X-rays. Herbig stars, such as MWC 480 and HD 163296, have bright photospheric UV emission, and thus the chemistry of these disks may be more sensitive to the stellar UV radiation field and any associated variations (such as accretion or jet variability; see Mendigutía et al. 2013; Francis et al. 2020; Rich et al. 2020). Unfortunately, with low degrees of observed variability and without concurrent X-ray or UV observations, we are unable to directly confirm the origin of the observed spectral variations.

Variations in the observed line emission could also be caused by changes in disk temperature instead of a change in molecular abundance. However, we find that the disk temperature—at least that in the mid-plane—remains constant to within the flux and rms error, as indicated by the continuum measurements. Additionally, if there were a change in disk temperature, the spectra would be universally and symmetrically scaled (assuming the flare uniformly impacts the disk; see, e.g., Favata et al. 2005), and the majority of variations in this work were found to occur asymmetrically on a channel-by-channel basis. Assuming that the $HCO^+$ 1–0 gas and continuum trace the same temperature regime, then spectral variations would most likely be due to changes in $HCO^+$ abundance, rather than temperature.

### 5.1.2. Possible Nonastrophysical Origins of Variability

Alternatively, the observed changes can be a product of how the disks were observed. Some examples include the following. (a) Because they are split out on a day-to-day basis, the data are naturally noisier than the final time-integrated image. Lower S/N, as is the case in the MWC 480 spectra, makes assessing low-level variability challenging.

(b) We minimized the effect of baseline coverage as much as possible (see Section 3.3 and Appendix A); however, baseline effects cannot be ruled out for HD 163296, the shift in AS 209 emission peak, or in IM Lup, because these instances of variability occurred when ALMA was in a compact configuration. Our flux recovery tests indicate that the variability in IM Lup was likely caused by spatial filtering, but HD 163296 and AS 209 variability likely has a different source.

(c) Flux calibrators are ideally considered to be constant on observationally relevant timescales, but this is not always the case. In reality, minor changes in flux calibrator luminosity do occur. If a flux calibrator varied in brightness, a symmetric and uniform change would be introduced in the $HCO^+$ spectra and continuum. The variations reported here are asymmetric and nonuniform (except for HD 163296). Therefore, we find that the changes in flux calibrator are an unlikely source of variability. For a complete list of flux calibrators used in this work, see Öberg et al. (2021).

### 5.2. Tentative First Detection of Spatial Variability in Disks

AS 209 and GM Aur are the first protoplanetary disks with potential spatial variability, as indicated by a shift in the spectral peak and variations in the line wings of the spectra. The physical origin of the peak shifts and fluctuations in spectral wings (if real) cannot be confirmed, due to the timing and limit of observation windows, but a reasonable explanation is that the shift was caused by an X-ray flare propagating through the disk. This discussion assumes an enhancement of $HCO^+$ immediately (within minutes) traces the flare, as indicated by Waggoner & Cleeves (2022).

Light produced by large X-ray flares (i.e., a flare that increases the characteristic luminosity by $>10\times$) will symmetrically propagate through the disk (due to the large size of the X-ray emitting region compared to the physical size of the star; see, e.g., Favata et al. 2005). If a disk were to be observed immediately after a flare occurs, i.e., after the flare hits the inner disk but has not yet reached the outer disk (hours after the flare), then an increase in inner disk $HCO^+$ emission would be seen. This effect would primarily be seen in the high-velocity spectral wings, as seen on 2019 September 3 for AS 209 and on 2019 August 31 for GM Aur.

If the disk were to be reobserved after the flare has propagated through the entire disk (over a timescale longer than the light-crossing time, i.e., ~days), then a uniform increase in the spectrum would be seen. A uniform enhancement occurred for $HCO^+$ in HD 163296 in this work and $H^{13}CO^+$ in IM Lup in Cleeves et al. (2017), suggesting that these observations occurred several days after the flare occurred.

After the flare has propagated through the entire disk, inner disk $HCO^+$ molecules will rapidly dissociate via electron recombination to H and CO, while the outer-disk $HCO^+$ abundance remains enhanced for a longer period, due to a lower level of free electrons. If $HCO^+$ rotational emission were observed during this time, the spectrum closer to the source velocity, including the peaks, would be enhanced while the wings would be quiescent. The spectra observed on 2018 October 26 for AS 209 and on 2019 September 2 for GM Aur are consistent with this interpretation. How flares change the chemistry as a function of radius and time is described further in Waggoner & Cleeves (2022), who report the same phenomena in models of $HCO^+$ column density throughout a flaring event (see Figure 7 in Waggoner & Cleeves 2022).

Large X-ray flares originating within extended stellar coronae are expected to uniformly illuminate the disk, changing the $HCO^+$ abundance across the entire azimuthal range. But this is not consistent with the type of variations seen in AS 209 and GM Aur. Because only half of the AS 209 spectrum is visible, due to cloud obstruction, we are unable to determine if the spectral changes were indeed spectrally (and spatially) symmetric. Future observations targeting warmer $HCO^+$ lines, which are expected to be less impacted by foreground absorption, are necessary to explore symmetric variations, as shown by Öberg et al. (2011) and Huang et al. (2017). GM Aur has a known $^{12}CO$ spiral structure (Huang

et al. 2021). When a flare occurs in this system, X-ray light would still uniformly propagate outward. Instead of uniformly impacting the disk and enhancing $HCO^+$, the flare could first impact the closest arm, thus causing an asymmetric increase in the $HCO^+$ spectrum. This cannot be confirmed without additional chemical modeling including 3D structure; however, both cases where $F_{HCO^+}$ increased in GM Aur only occurred in the redshifted portion of the spectrum.

### 5.3. Tentative First Detection of Variability in a Herbig System

We report the first tentative detection of $HCO^+$ variability in a Herbig protoplanetary disk system, HD 163296. Unfortunately, the peak $HCO^+$ emission occurred during the first observation window, and the following observation windows did not occur until a year later. If HD 163296's enhancement was real, the duration and behavior are unknown because it was not reobserved for nine months. Thus, it is challenging to determine the exact cause of $HCO^+$ variability in this source. While the source of variability could be an X-ray flare, it is also possible that a fluctuation of UV radiation could have led to the higher $HCO^+$ emission observed in 2018 October.

Fluctuations in UV flux may be a more likely origin than X-rays in HD 163296, as Herbig stars are more massive and hotter than solar-mass T Tauri stars. Stellar spectrum for Herbig star emission peaks in the UV range, resulting in much lower relative contributions from X-ray emission than T Tauri stars. Therefore, Herbig disk ionization may instead be driven by a variable UV flux. Because $HCO^+$ is sensitive to disk ionization rates, which are connected to both UV and X-ray flux (e.g., Seifert et al. 2021), it is impossible to determine the exact origin of variability in HD 163296 without further multiwavelength monitoring observations.

### 5.4. Comparison to X-Ray Flare Models

How does the degree of $HCO^+$ variability compare with that predicted by chemical models including X-ray flares? Of the five sources observed by MAPS, none showed strong variability at the level previously seen in IM Lup, as reported in Cleeves et al. (2017). X-ray flares are known to occur on a regular basis (varying by factors of 4–10 about once a week for T Tauri stars; see Wolk et al. 2005). Stronger flares are rarer; they occur only every few months (varying by factors greater than 10).

We can compare this lack of strong chemical variability with disk models reported in Waggoner & Cleeves (2022). Based on the typical uncertainty in the measured disk-integrated flux, a minimum change of *at least* 100% in disk-integrated $F_{HCO^+}$ is required to confidently detect enhancement ($>3\sigma$). A smaller change may be detectable in a disk with a higher S/N, but this discussion uses the typical flux and uncertainties in this work. Flare models predict a 2.2% chance of observing the disk-integrated $HCO^+$ enhanced by a factor of at least 100% when observed one time on any given day. Each of the MAPS disks was observed between three and six times, so we can estimate the probability that they are observed to be enhanced during at least one of these observations.

In total, 24 separate observations were executed. If this entire data set is considered, then there is a 41% chance of observing clear and distinguishable variability. If Herbig (observed 11 times) and T Tauri systems (observed 13 times) are considered separately, then the chances of observing enhancement are only

22% and 25%, respectively. For the HD 163296 disk (observed six times), there was a 12.5% chance of observing $HCO^+$ to be enhanced by 100% or greater at least one time. For the disks observed five times, AS 209, GM Aur, or MWC 480, there was a 10.5% chance of observing them with elevated $HCO^+$. Finally, IM Lup was only observed three times, and thus there is a 6.5% chance of observing variability in IM Lup.

We note that the theoretical probabilities discussed here are likely an overestimate of the chance of detecting a flare, because many of the MAPS observations occurred within several days with each other, while the modeled statistics are derived from a 500 yr window and assume observations are independent. This discussion also assumes $HCO^+$ emission increases linearly with an increase in abundance, which is only true if the line is optically thin and the emitting conditions are constant. Additionally, these statistics are true for X-ray flares produced by T Tauri stars, and the probability of observing X-ray or UV-driven variability in a Herbig star is likely different.

## 6. Conclusions

Fluctuations in ionization, such as an X-ray flaring event, have been shown to temporarily increase the abundance of gas-phase cations, which results in time-variable emission. In this work, we searched for variability in $HCO^+$ $J = 1-0$ in the HD 163296, AS 209, GM Aur, MWC 480, and IM Lup protoplanetary disks using data from the MAPS ALMA Large Program. While disk-integrated $F_{HCO^+}$ remained constant within the uncertainty across all observations, low-level spectral variability was seen in all five disks.

1. AS 209: On 2018 October 26, the $HCO^+$ spectral peak is increased and shifted blueward toward the source velocity. While this particular shift could be impacted by baseline coverage, there is also variation in the spectral wings, and an increase in blueshifted emission is also seen on 2019 September 3.
2. GM Aur: There is an asymmetric increase in peak emission on 2019 September 2, and enhancement in the redshifted wing is also seen on 2019 August 31. The asymmetric spectral shifts may be due to disk structural asymmetry, as GM Aur has spiral arms in $^{12}CO$ gas emission.
3. HD 163296: The spectral peaks are slightly enhanced on 2018 October 22 compared to later observations. While this could be due to an increase in ionization rates, this fluctuation could also be due to varying baseline coverage.
4. IM Lup: There is an asymmetric increase in emission for the redshifted peak on 2019 August 21, but this same phenomenon occurs in data simulated using `vis_sample`. Therefore, the spectral variation in IM Lup is most likely introduced by differences in baseline coverage between observations.
5. MWC 480: There is a change in spectral shape on 2019 September 4, where the spectrum has a single peak compared to two peaks on the other observation days. However, the change in shape can be attributed to higher levels of noise and is not conclusively astrophysical.

Our observations are consistent with the theory that a temporary increase in high-energy stellar emission can drive changes in the abundance and flux of gas-phase cations in planet-forming disks (Waggoner & Cleeves 2022).

Additionally, we show that substantial serendipitous fluctuations in disk-integrated flux such as were seen in IM Lup (Cleeves et al. 2017) are rare. In order to confidently detect flare-driven chemistry and constrain spectral variation, a dedicated time-domain campaign, optimizing high S/N, is required. A designated time-domain observing program is necessary to measure variable gas-phase cation emission. Such a program will be scientifically useful, as it could result in measurements of electron abundances and information about magnetic fields, magnetorotational instability, and disk accretion (e.g., Balbus & Hawley 1991; Glassgold et al. 1997; Ilgner & Nelson 2006b).

## Appendix A
## Visibility Effects on HCO$^+$ Emission

To ensure that any detected variability was not artificially introduced by varying telescope configurations, the Python function `vis-sample` was used to generate "mock" data (as described in Section 3.3). These data are produced using the exact same CLEANing method as the real data. Therefore, the mock data reveal any variability that would have been introduced by varying baseline coverage from different telescope configurations (Figure 8).

IM Lup is the only system with a clear baseline effect in the mock data. $F_{HCO^+}$ on 2019 August 21 is higher than the other observations, despite the fact that all mock observations were modeled using the same initial measurement set. This same effect is seen in the real data (Figure 6), and it is attributed to baseline coverage.

There are several scenarios where observations with more complete short-baseline coverage (i.e., those taken in 2018 October) yield slightly higher $F_{HCO^+}$ values (HD 163296, AS 209). In the disks where this effect occurs, no significant variations were seen in the mock line or continuum flux. There are variations in the disk-integrated flux values, most notably in $F_{cont}$. This variation is attributed to rms uncertainty, because all $F_{cont}$ values are with $\pm 10\%$ of each other (see Section 4.2). Changes in flux are unlikely to be caused by baseline coverage.
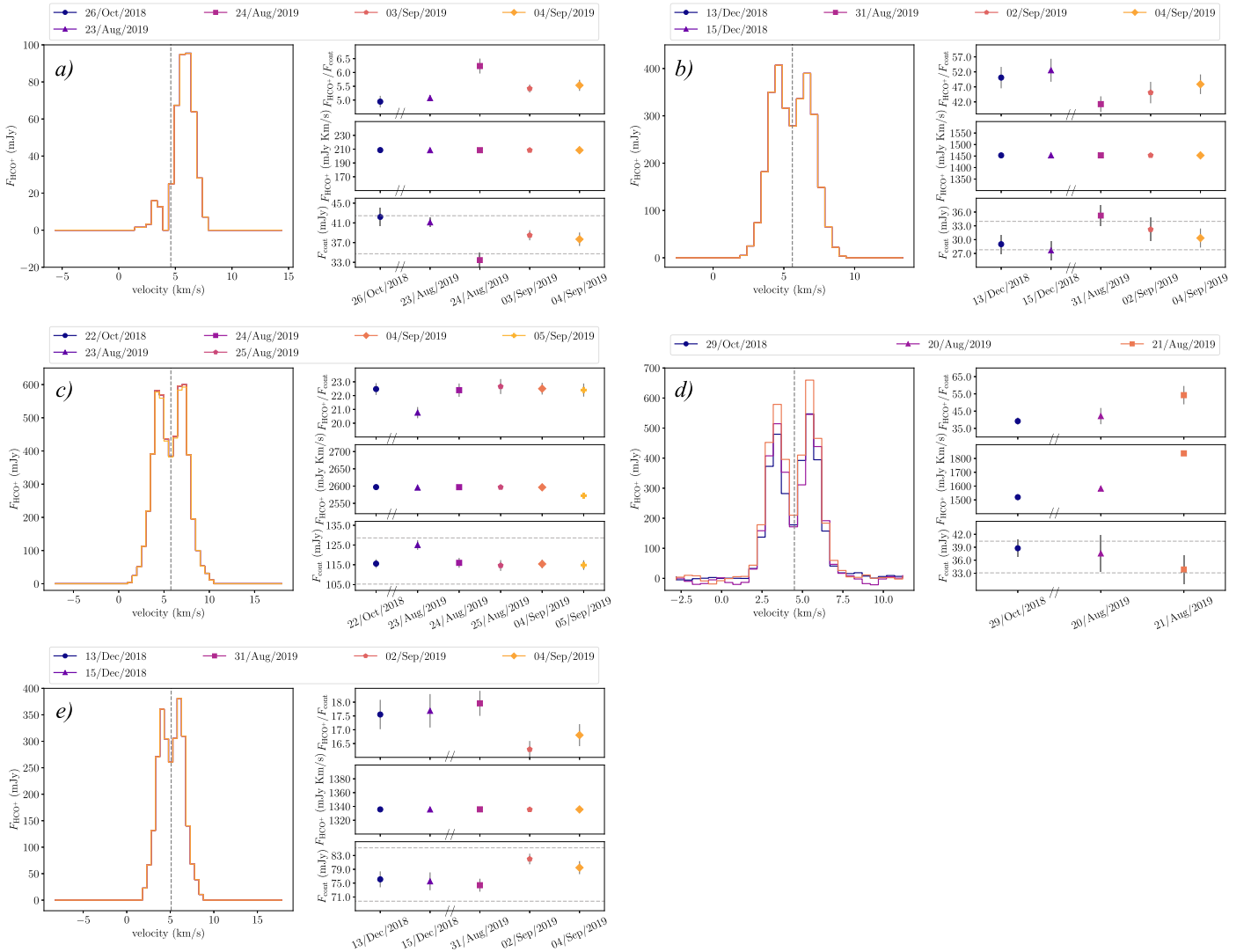
**Figure 8.** Synthetic spectra ("mock data") produced using the `vis-sample` routine on the time-integrated HCO$^+$ 1–0 cubes. These models reveal any spectral or flux fluctuations that would have been introduced by varying baseline coverage for each source's unique spatial emission structure. The subfigures show the respective analyses for (a) AS 209, (b) GM Aur, (c) HD 163296, (d) IM Lup, and (e) MWC 480. For each panel, the mock HCO$^+$ 1–0 spectrum is shown on the left, and the mock disk-integrated continuum, line, and continuum normalized line emission are shown on the right. It should be noted that the spectra overlap.

## Appendix B
## Channel Error Bars on Spectra

All spectral changes reported in this work are considered tentative because no change is $>3\sigma$. However, there are a number of spectral variations greater than the level of noise, as shown in Figure 9 and defined as follows.

1. AS 209: The peak at $6.1\,\mathrm{km\,s^{-1}}$ is enhanced and shifted toward source velocity on 2018 October 26. The $6.1\,\mathrm{km\,s^{-1}}$ peak appears to also be shifted and enhanced on 2019 September 4, but not above the level of noise, so it is not considered a change in emission in this work. On most observation days, little to no blueshifted emission is seen, except on 2019 September 3.

2. GM Aur: The peak at $6.6\,\mathrm{km\,s^{-1}}$ is enhanced on 2018 October 26, and a shoulder is visible at $9.6\,\mathrm{km\,s^{-1}}$ on 2019 September 2.
3. HD 163296: Both central peaks are enhanced on 2018 October 22 compared to the following observations.
4. IM Lup: The peak at $6.8\,\mathrm{km\,s^{-1}}$ is enhanced on 2019 August 21 compared to the other two observations.
5. MWC 480: An unknown emission peak is seen on 2019 September 4 at $-2.4\,\mathrm{km\,s^{-1}}$ and not on any other observation day. There may be a shift in spectral shape on 2019 September 4, but the change is below the level of noise and not considered in this work.

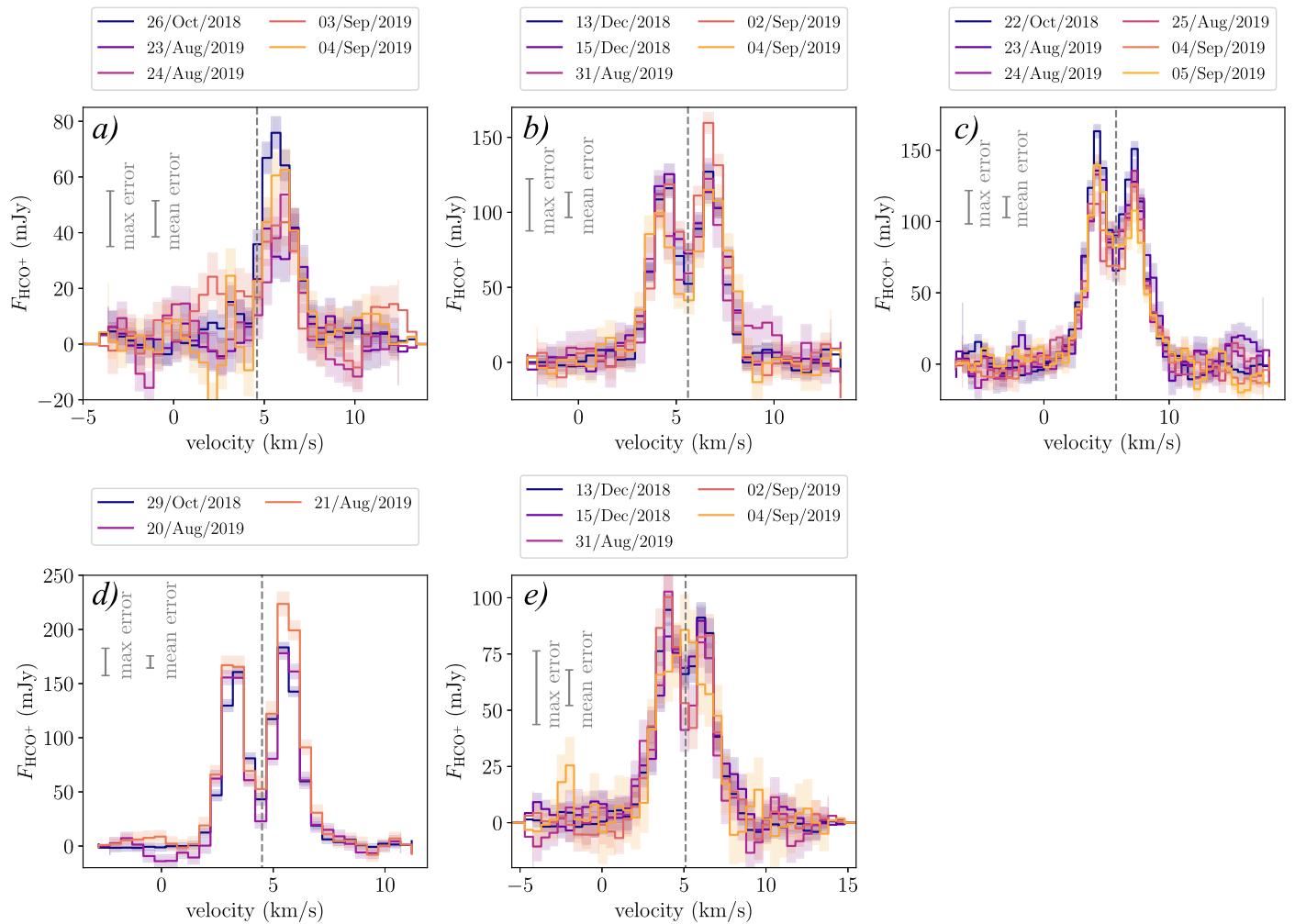For more information on error calculations, see Section 3.2.

**Figure 9.** HCO$^+$ $J = 1$–0 spectra for each of the MAPS disks with error bars for each channel. The gray error bars represent the max and mean error bars (standard deviation) for all channels. (a) AS 209. (b) GM Aur. (c) HD 163296. (d) IM Lup. (e) MWC 480.

## ORCID iDs

Abygail R. Waggoner https://orcid.org/0000-0002-1566-389X

L. Ilsedore Cleeves https://orcid.org/0000-0003-2076-8001

Ryan A. Loomis https://orcid.org/0000-0002-8932-1219

Yuri Aikawa https://orcid.org/0000-0003-3283-6884

Jaehan Bae https://orcid.org/0000-0001-7258-770X

Jennifer B. Bergner https://orcid.org/0000-0002-8716-0482

Alice S. Booth https://orcid.org/0000-0003-2014-2121

Jenny K. Calahan https://orcid.org/0000-0002-0150-0125

Gianni Cataldi https://orcid.org/0000-0002-2700-9676

Charles J. Law https://orcid.org/0000-0003-1413-1776

Romane Le Gal https://orcid.org/0000-0003-1837-3772

Feng Long https://orcid.org/0000-0002-7607-719X

Karin I. Öberg https://orcid.org/0000-0001-8798-1347

Richard Teague https://orcid.org/0000-0003-1534-5186

David J. Wilner https://orcid.org/0000-0003-1526-7587

## References

Aikawa, Y., Cataldi, G., Yamato, Y., et al. 2021, ApJS, 257, 13
Avenhaus, H., Quanz, S. P., Garufi, A., et al. 2018, ApJ, 863, 44
Balbus, S. A., & Hawley, J. F. 1991, ApJ, 376, 214
Benz, A. O., & Güdel, M. 2010, ARA&A, 48, 241
Cleeves, L. I., Bergin, E. A., Öberg, K. I., et al. 2017, ApJL, 843, L3
Cortes, P., Remijan, A., Carpenter, J., et al. 2022, ALMA Cycle 9 Technical Handbook (ALMA Doc. 9.3, ver. 1.0), Zenodo, doi:10.5281/zenodo.7764458
Czekala, I., Loomis, R. A., Teague, R., et al. 2021, ApJS, 257, 2
Espaillat, C. C., Macías, E., Wendeborn, J., et al. 2022, ApJ, 924, 104
Favata, F., Flaccomio, E., Reale, F., et al. 2005, ApJS, 160, 469
Favre, C., Fedele, D., Maud, L., et al. 2019, ApJ, 871, 107
Feldman, U., Doschek, G. A., & Klimchuk, J. A. 1997, ApJ, 474, 511
Fischer, W. J., Hillenbrand, L. A., Herczeg, G. J., et al. 2022, arXiv:2203.11257
Francis, L., Johnstone, D., Herczeg, G., Hunter, T. R., & Harsono, D. 2020, AJ, 160, 270
Getman, K. V., Akimkin, V. V., Arulanantham, N., et al. 2022a, RNAAS, 6, 64
Getman, K. V., & Feigelson, E. D. 2021, ApJ, 916, 32
Getman, K. V., Feigelson, E. D., Garmire, G. P., et al. 2022b, ApJ, 935, 43
Getman, K. V., Flaccomio, E., Broos, P. S., et al. 2005, ApJS, 160, 319
Glassgold, A. E., Najita, J., & Igea, J. 1997, ApJ, 480, 344
Grady, C. A., Hamaguchi, K., Schneider, G., et al. 2010, ApJ, 719, 1565
Güdel, M. 2004, A&ARv, 12, 71
Güdel, M., Audard, M., Kashyap, V. L., Drake, J. J., & Guinan, E. F. 2003, ApJ, 582, 423
Henning, T., & Semenov, D. 2013, ChRv, 113, 9016
Huang, J., Andrews, S. M., Dullemond, C. P., et al. 2020, ApJ, 891, 48
Huang, J., Bergin, E. A., Öberg, K. I., et al. 2021, ApJS, 257, 19
Huang, J., Öberg, K. I., & Andrews, S. M. 2016, ApJL, 823, L18
Huang, J., Öberg, K. I., Qi, C., et al. 2017, ApJ, 835, 231
Ilgner, M., & Nelson, R. P. 2006a, A&A, 455, 731
Ilgner, M., & Nelson, R. P. 2006b, A&A, 445, 223
Kóspál, Á., Cruz-Sáenz de Miera, F., White, J. A., et al. 2021, ApJS, 256, 30
Law, C. J., Loomis, R. A., Teague, R., et al. 2021, ApJS, 257, 3

Leemker, M., van't Hoff, M. L. R., Trapman, L., et al. 2021, A&A, 646, A3
Loomis, R. A., Cleeves, L. I., Öberg, K. I., et al. 2018, ApJ, 859, 131
Maloney, P. R., Hollenbach, D. J., & Tielens, A. G. G. M. 1996, ApJ, 466, 561
Mendigutía, I., Brittain, S., Eiroa, C., et al. 2013, ApJ, 776, 44
Molyarova, T., Akimkin, V., Semenov, D., et al. 2018, ApJ, 866, 46
Öberg, K. I., & Bergin, E. A. 2021, PhR, 893, 1
Öberg, K. I., Guzmán, V. V., Walsh, C., et al. 2021, ApJS, 257, 1
Öberg, K. I., Qi, C., Fogel, J. K. J., et al. 2010, ApJ, 720, 480
Öberg, K. I., Qi, C., Fogel, J. K. J., et al. 2011, ApJ, 734, 98
Panić, O., Hogerheijde, M. R., Wilner, D., & Qi, C. 2009, A&A, 501, 269
Pearce, G., & Harrison, R. A. 1988, A&A, 206, 121
Piétu, V., Dutrey, A., & Guilloteau, S. 2007, A&A, 467, 163
Pinte, C., Ménard, F., Duchêne, G., et al. 2018, A&A, 609, A47

Rich, E. A., Wisniewski, J. P., Sitko, M. L., et al. 2020, ApJ, 902, 4
Ruíz-Rodríguez, D. A., Williams, J. P., Kastner, J. H., et al. 2022, MNRAS, 515, 2646
Seifert, R. A., Ilsedore Cleeves, L., Adams, F. C., & Li, Z.-Y. 2021, ApJ, 912, 15
Teague, R., Bae, J., Aikawa, Y., et al. 2021, ApJS, 257, 18
Teague, R., Bae, J., & Bergin, E. A. 2019, Natur, 574, 378
Thompson, A. R., Moran, J. M., & Swenson, G. W., Jr. 2017, Interferometry and Synthesis in Radio Astronomy (3rd ed.; Cham: Springer)
Tobin, J. J., van't Hoff, M. L. R., Leemker, M., et al. 2023, Natur, 615, 227
Waggoner, A. R., & Cleeves, L. I. 2019, ApJ, 883, 197
Waggoner, A. R., & Cleeves, L. I. 2022, ApJ, 928, 46
Wolk, S. J., Harnden, F. R., Jr., Flaccomio, E., et al. 2005, ApJS, 160, 423